Supporting Information
Mechanism of the Acyl–Enzyme Complex Formation from the Henry–Michaelis Complex of Class C β–Lactamases with β–Lactam Antibiotics

Ravi Tripathi and Nisanth N. Nair[*1]

Department of Chemistry

Indian Institute of Technology Kanpur, 208016 Kanpur, India

1 Details of Modeling the Aztreonam–CBL complex

Starting structure of the β-lactamase with aztreonam was taken from the *C freundii* class C enzymes complexed with reacted aztreonam molecule (PDB 1FR6). [1] The coordinates of the reacted aztreonam molecule were extracted from acyl-enzyme structure (PDB:1FR6), superposed with the apoenzyme structure (PDB: 1FR1). The β-lactam ring of aztreonam molecule was modeled using the `molden` software [2] and optimized with HF/6-31G* using the Gaussian09 suite of program.[3] The coordinates of the aztreonam molecule (with optimized β-lactam ring) were provided in the 1FR1 structure and this structure was used as the starting structure for further MD simulations.

2 Protonation States of the Amino Acid Side Chains

Two different side chain protonation states for Lys_{67} and Tyr_{150} were considered in this work; see Figure 2 of the manuscript. For the residues other than Lys_{67} and Tyr_{150} was

[1*] Corresponding Author: nnair@iitk.ac.in

based on their standard pK_a values at pH 7. Aspartic and glutamic acid residues were considered in their deprotonated state, based on the pK_a obtained from the H++ server. [4] The histidine residues were protonated at the N_ϵ position, based on its contact in the X-ray structure.

3 Definition of Coordination Number Collective Coordinate

Coordination number of A atom with a group of B atoms, $C[\mathrm{A}-\mathrm{B}]$, is defined by the analytical function

$$C[\mathrm{A}-\mathrm{B}] = \sum_{J\in \mathrm{B}} \frac{1}{1+\left(\frac{d[\mathrm{A}-J]}{d^0_{\mathrm{AB}}}\right)^6} \tag{1}$$

where d^0_{AB} is a parameter chosen based on the van der Waals parameters of the atoms involved. When the internuclear distance $d[\mathrm{A}-J]$ between atom A and I is more than d^0_{AB}, the fraction inside the sum is close to 1, else close to zero. The value of the parameter d^0_{AB} for various coordination number CCs are listed in Table SI 1.

Table SI 1

CCs	d^0_{AB}
CC1	1.35
CC3	1.37
CC6	1.80
CC7	1.37
CC10	1.37
CC11	1.94, 1.94

4 Transition Path Sampling

We started TPS from $\mathbf{TS}_{4-5}$ located on the reconstructed free energy surface, as obtained from the metadynamics simulation. Out of the total fourteen trajectories eight trajectories have proceeded to the intermediate **5** and the remaining proceeded to the reactant minimum **4**. Similarly, on performing another TPS from $\mathbf{TS}_{5-6}$, out of the fourteen trajectories seven of them have advanced to the intermediate **5** while the remaining progressed to the product **6**; see the Fig SI 1 and Fig SI 2.

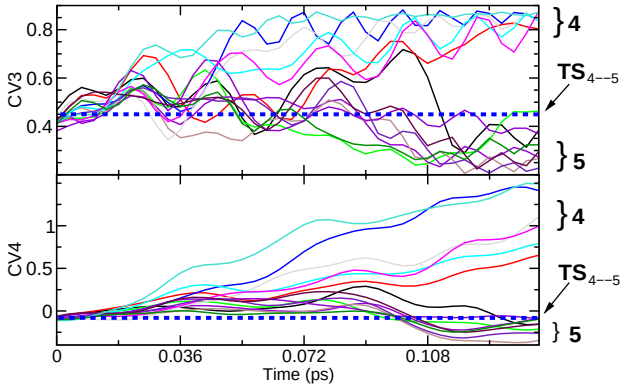

Fig SI 1: The plot of CV3 and CV4 along the trajectories after TPS from the saddle point $\mathbf{TS}_{4-5}$

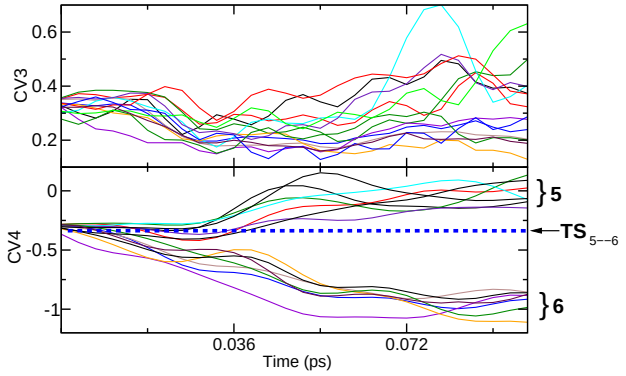

Fig SI 2: The plot of CV3 and CV4 along the trajectories after TPS from the saddle point $\mathbf{TS}_{5-6}$

5 PBE Error Analysis

In order to check the accuracy of the PBE functional used in our calculations, we have compared the potential energy barrier computed for the **1**→**2**, **1**→**3**, **4**→**5**, and **5**→**6** processes, using PBE and M06–2X [5] functionals. The latter functional is known for their accuracy in computing the barrier heights. All the calculations were performed with Gaussian09 [3] suite of program. 6-31++G(d) basis set was used for these calculations. Truncated structures resembling **1** for aztreonam and **3** and **4** for cephalothin, were taken as the reference for the reactant structures. The models used for **1**→ **2** and **1**→ **3** comprised of 101 atoms, whereas those used for **4**→**5** and **5**→**6** contained 116 atoms. The side chains of Ser_{64}, Lys_{67}, Asn_{152}, Glu_{272}, Lys_{315}, Thr_{316} and Ser_{318}/Ala_{318} residues and truncated Cep and Azt were included in the model: see also Fig SI 3 and 4 The structures correspond to transition states ($\mathbf{TS}_{1-2}$), ($\mathbf{TS}_{1-3}$), ($\mathbf{TS}_{4-5}$) and ($\mathbf{TS}_{5-6}$) were modeled using the molden software. (See Fig SI 3 and 4). Single point calculations were performed for reactant and TS structures separately, for all the four processes. The computed potential energy barriers are given in SI Table 2.

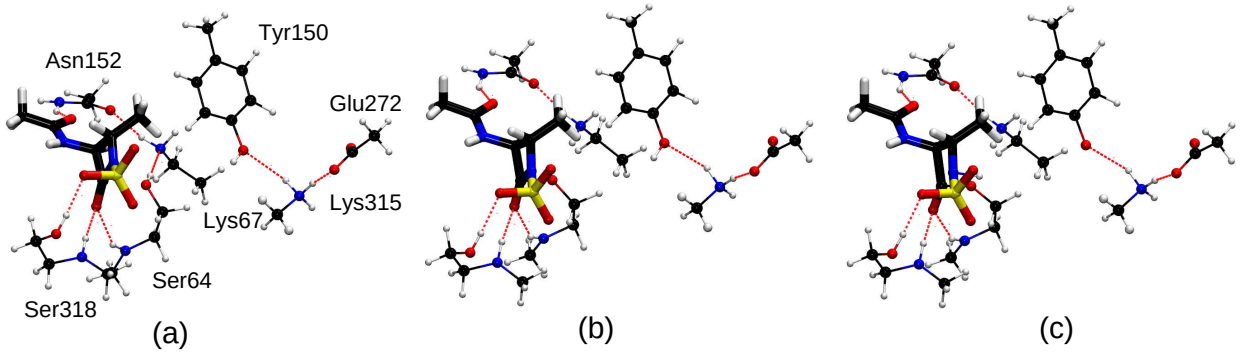

Fig SI 3: Truncated model used for the error analysis: (a) Reactant (**1**); (b) Transition state ($\mathbf{TS}_{1-2}$); (c) Transition state ($\mathbf{TS}_{1-3}$)

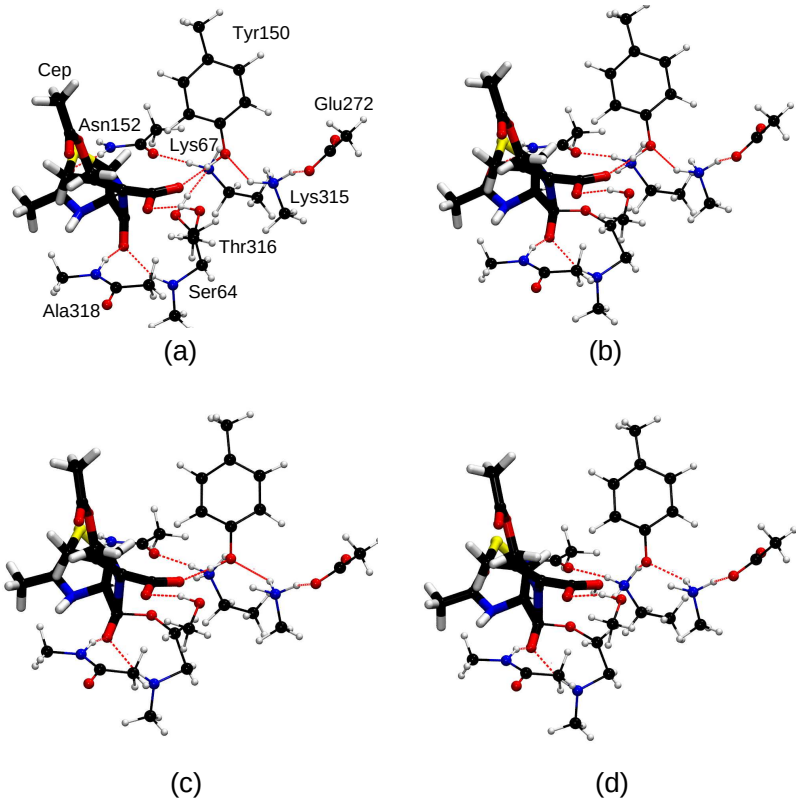

Fig SI 4: Truncated model used for the error analysis: (a) Reactant (**4**); (b) Transition state ($\mathbf{TS}_{4-5}$); (c) Intermediate (**5**); (d) Transition state ($\mathbf{TS}_{5-6}$)

Table SI 2: Potential energy barrier $\Delta U^{\ddagger}$ (kcal/mol) calculated for the truncated models with PBE, and M06–2X functionals.

Reaction	$\Delta U^{\ddagger}$		Error
	PBE	M06–2X	$(\Delta U^{\ddagger}_{\mathrm{PBE}} - \Delta U^{\ddagger}_{\mathrm{M06-2X}})$
1→ **2**	38.65	39.47	−0.82
1→ **3**	26.90	28.98	−2.08
4→ **5**	39.63	42.34	−2.71
5→ **6**	25.85	24.43	+1.42

6 RMSD Plots

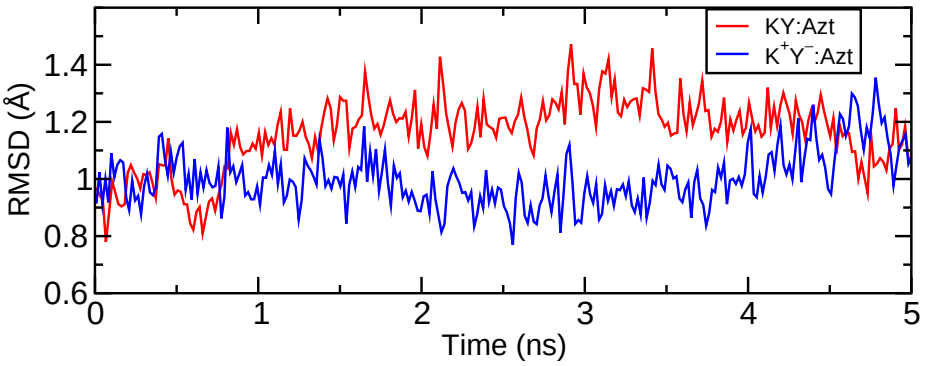

Fig SI 5: Backbone RMSD along the NVT simulation of CBL with respect to the starting structure for **KY:Azt** (red) and **K$^+$Y$^-$:Azt**- (blue).

7 Selected Interactions within the Active Site of CBL–Drug Non–Covalent Complexes

Table SI 3: Average distance (in Å) between selected atoms in the active site of various equilibrium structures of CBL–drug noncovalent structures computed from the empirical force–field MD simulation; standard deviations are shown in the brackets.

Distance	**KY:AztA**	**KY:AztB**	**K^+Y^-:Azt**	**K^+Y^-:Cep**	**KY:Cep**
$Tyr_{150}O_\eta \cdots Lys_{67}N_\zeta$	4.53 (0.39)	3.76 (0.31)	2.91 (0.17)	2.98 (0.20)	2.89 (0.31)
$Tyr_{150}O_\eta \cdots Lys_{315}N_\zeta$	3.06 (0.23)	2.98 (0.17)	2.85 (0.11)	2.81 (0.09)	3.01 (0.17)
$Lys_{67}N_\zeta \cdots Asn_{152}O_\delta$	2.93 (0.15)	2.98 (0.18)	2.83 (0.13)	2.97 (0.24)	2.91 (0.13)
$Lys_{67}N_\zeta \cdots Ala_{220}O$	3.04 (0.21)	4.87 (0.39)	4.62 (0.38)	4.60 (0.37)	4.49 (0.43)
$Lys_{315}N_\zeta \cdots Glu_{272}O_\epsilon 1$	2.73 (0.10)	2.79 (0.20)	3.02 (0.22)	3.07 (0.21)	2.97 (0.18)
$Lys_{315}N_\zeta \cdots Glu_{272}O_\epsilon 2$	2.73 (0.10)	2.79 (0.20)	2.82 (0.15)	2.83 (0.13)	2.91 (0.16)
$Ser_{64}O_\gamma \cdots AztC_2$	3.27 (0.24)	3.17 (0.17)	3.33 (0.23)	–	–
$Ser_{64}O_\gamma \cdots CepC_8$	–	–	–	3.02 (0.12)	2.96 (0.13)

8 Active Site Structures of KY:AztA and KY:AztB Conformers

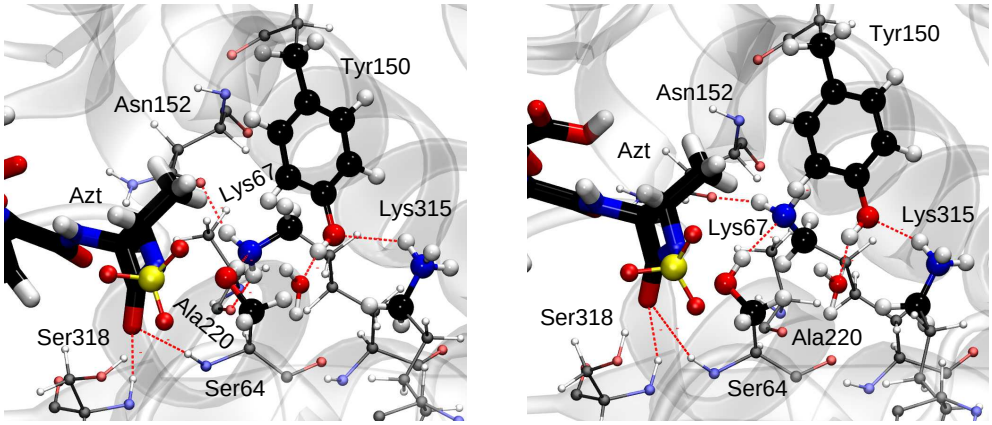

Fig SI 6: Equilibrated active site structure of (a) **KY:AztA** and (b) **KY:AztB**

9 Metadynamics Simulation of 2→1

To determine the free energy barrier of process **2** → **1**, we performed a metadynamics calculation starting with structure **2**. We chose 2 CCs: (a) coordination number of $Ser_{64}O_{\gamma}$ to $Ser_{64}H_{\gamma}$ (CC8); (b) distance difference $d[Ser_{64}O_{\gamma}–Azt_{362}C_2]–d[Azt_{362}C_2–Azt_{362}N_1]$ (CC2). A wall at –0.3 Å was applied on the second CV to avoid the sampling of structure **3**. The free energy barrier for this process was estimated to be 2 kcal mol^{-1}. The reconstructed free energy surface has shown in Fig SI 7

10 Metadynamics Simulation of 5→4

A similar metadynamics calculation, as above, has been performed to determine the free energy barrier for **5** → **4** process. Two CCs have been chosen (a) coordination number of $Ser_{64}O_{\gamma}$ to $Ser_{64}H_{\gamma}$(CC8); (b) distance difference $d[Ser_{64}O_{\gamma}–Cep_{362}C_8]–d[Cep_{362}C_8–Cep_{362}N_5]$(CC4). A wall at -0.3 Å was applied on the second CV to avoid the **5→6** transformation. The

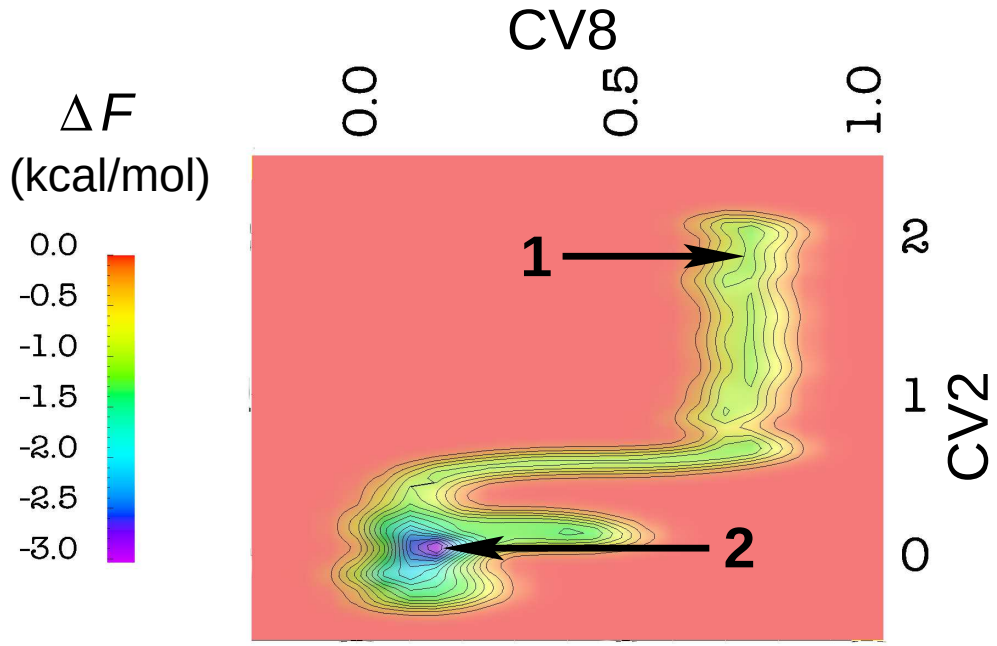

Fig SI 7: Reconstructed free energy surface for reaction **2** → **1**. CV8 and CV2 corresponds to the collective variables coupled to CC8 and CC2. Here CC2 is in Å.

reconstructed free energy surface is shown in Fig SI 8. The free energy barrier for **5**→**4** is only 2 kcal mol^{-1}.

11 Metadynamics Simulation to Test Tyr$_{150}$ as Base Starting with the K$^+$Y$^-$:Azt Structure

To check the possibility of Tyr$_{150}$ acting as a base for the acylation reaction of aztreonam, we carried out metadynamics simulation with a structure in the **K$^+$Y$^-$:Azt** protonation state.

A suitable initial structure was chosen from the empirical force–field simulation of **K$^+$Y$^-$:Azt**, and is shown in Fig SI 9. Interestingly, during the 2 ps QM/MM simulation (performed prior to metadynamics), we observed frequent proton transfer between Ser$_{64}$ and Tyr$_{150}$ in concomitant with proton transfer between Lys$_{67}$ and Ser$_{64}$: i.e. interconversion of **K$^+$Y$^-$:Azt** and **KY:Azt** protonation states (see Fig SI 9). We have then carried

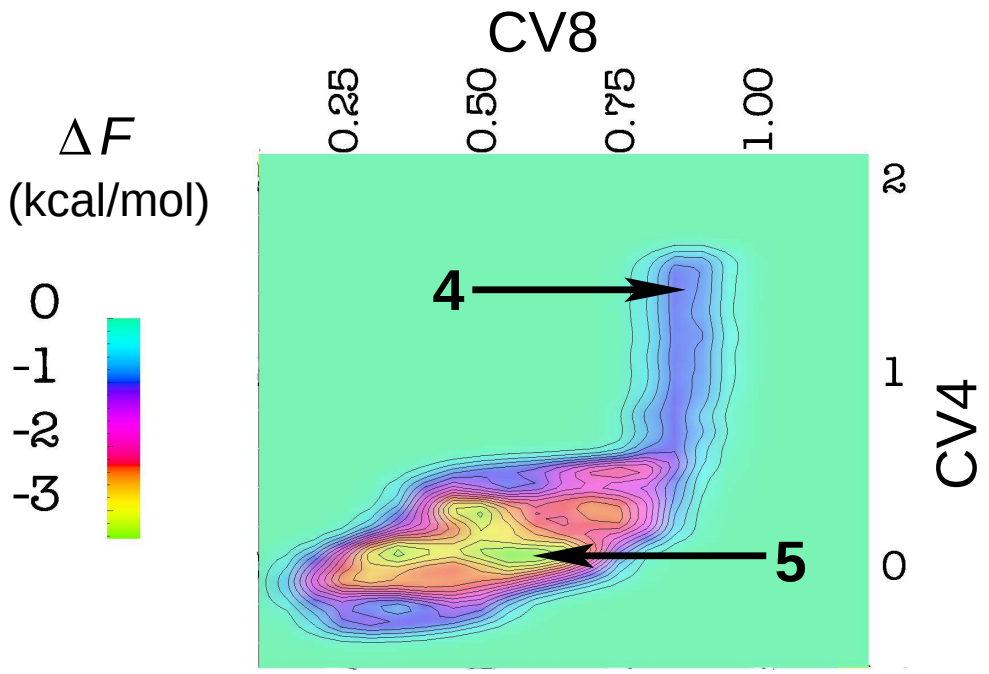

Fig SI 8: (a) Reconstructed free energy surface for reaction **5**→**4**. Here CC4 is in Å.

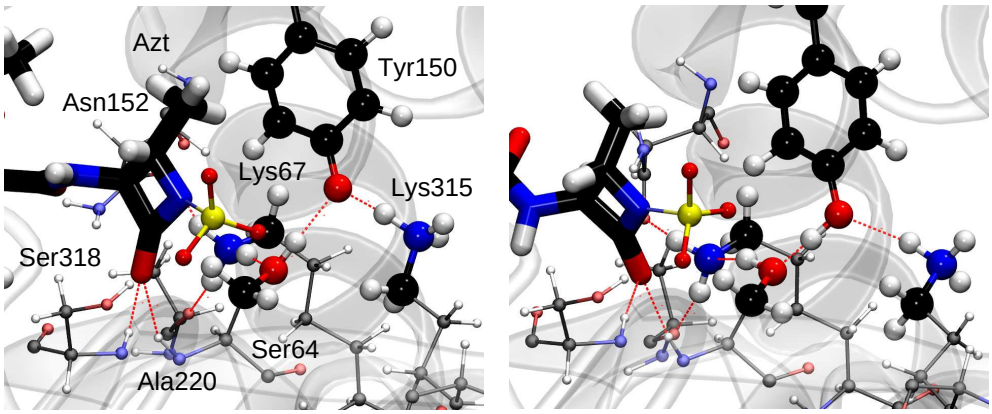

Fig SI 9: Snapshots from the QM/MM simulation as described in Section 11: a) $\mathbf{K^+Y^-}$**:Azt** and b) **KY:Azt** conformers

out the metadynamics simulation with the **K$^+$Y$^-$:Azt** conformer, but by constraining Lys_{67} to be in the protonated form. Two CCs were chosen for the metadynamics simulation: (a) coordination number of $Ser_{64}H_\gamma$ to $Tyr_{150}O_\eta$ (CC10) and (b) the coordination number difference, C[$Ser_{64}O_\gamma$−$Azt_{362}C_2$]–C[$Azt_{362}C_2$−$Azt_{362}N_1$] (CC11). The simulation was continued till 38 kcal/mol of free energy was filled in the reactant basin. As clear from Fig SI 10, the acylation reaction was not observed (See Fig SI 10). Partial proton transfers were seen between Ser_{64} and Tyr_{150}, but it was not leading to the acylation. From this data, we can conclude that Tyr_{150} can not act as the general base during the acylation of aztreonam.

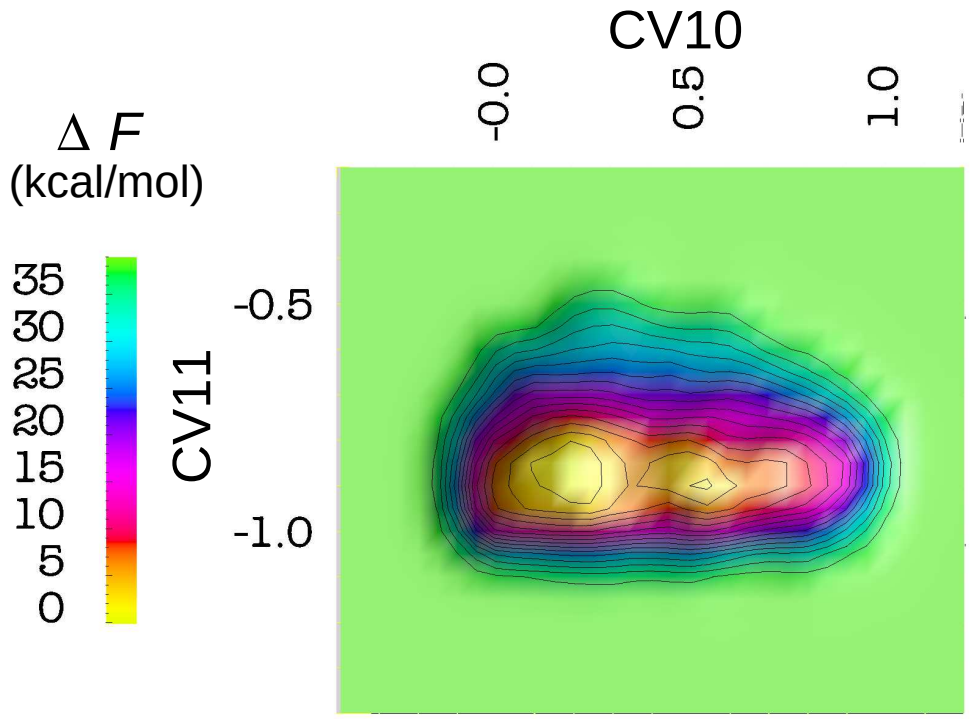

Fig SI 10: Reconstructed free energy surface starting with **K$^+$Y$^-$:Azt** protonation state.

12 Modeling Acylation Reaction using KY:AztA

12.1 Reconstructed Free Energy Surface

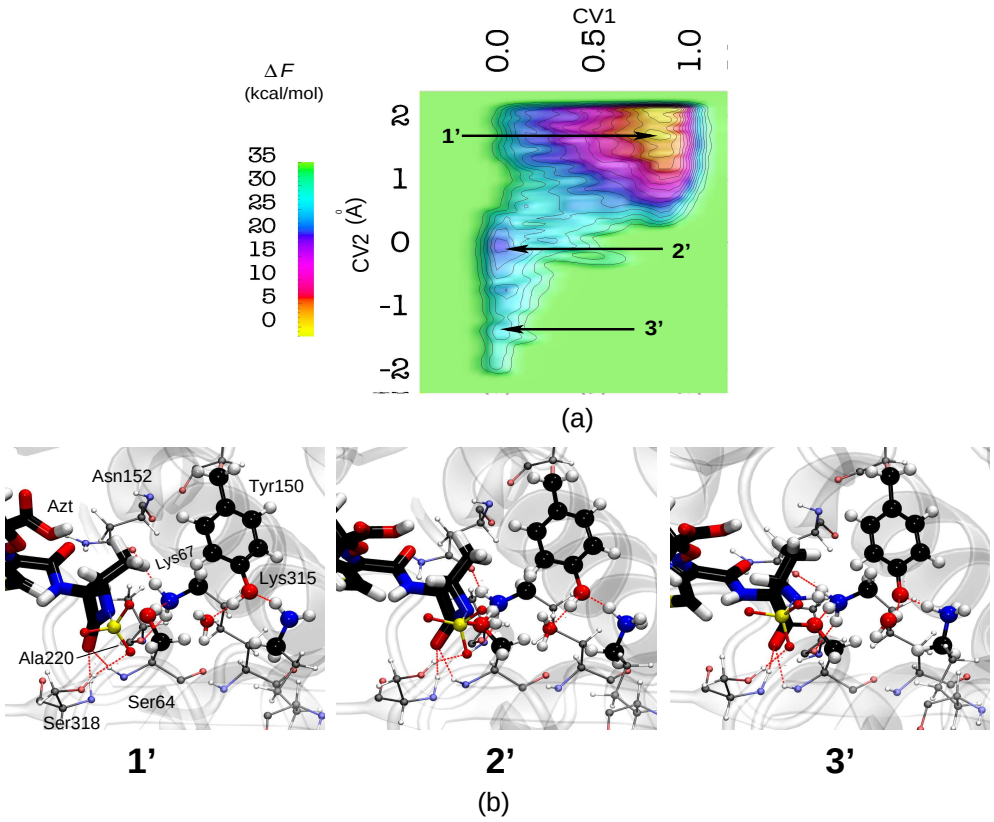

Fig SI 11: (a) Reconstructed free energy surface, (b) snapshots, for the acylation reaction, starting with structure **KY:AztA**, of CBL with aztreonam. The structures **1'**, **2'** and **3'** differ from structures **1**, **2** and **3**, respectively, by the relative orientation of Lys_{67}. See the main manuscript for details and also SI Section 12.2.

12.2 Modeling 3′ to 3

Here we study the formation of **3** (product configuration in the metadynamics simulation using **KY:AztB**) from **3′** (product configuration observed soon after the metadynamics simulation of acylation using **KY:AztA**). An empirical force field simulation has been performed starting with the product structure **3'** to this structural change. [2] During the empirical force field simulation (NPT), we observed that the hydrogen bond between Lys_{67} and Ala_{220} breaks and Lys_{67} rotates toward Tyr_{150}, resulting in **3**. The conformer **3** was the major structure in the 1 ns NPT simulation. This indicates that the final structures of **KY:AztA** and **KY:AztB** metadynamics simulation converge to the identical final state **3**.

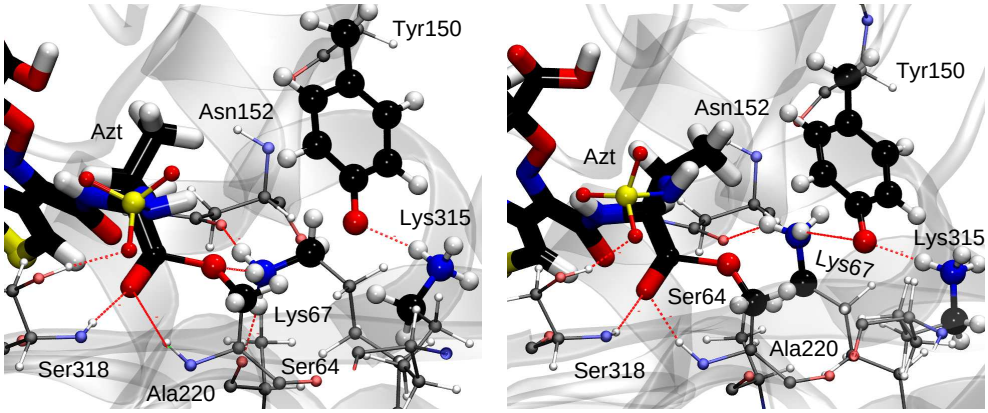

Fig SI 12: Snapshots of the active site structure of (a) structure **3'** and (b) structure **3**, seen during 1 ns of MD simulation.

[2]The RESP charges of acylated aztreonam and complexed Ser_{64} were calculated using RED software. GAFF force field was used to define the parameter of the aztreonam–Ser_{64} complex.

13 Configurations Sampled during the Metadynamics Simulation of Acylation of Cephalothin

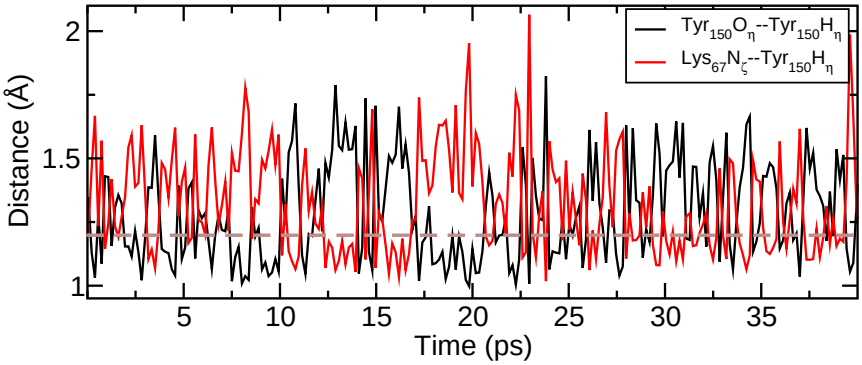

Fig SI 13: Distances $\mathrm{Tyr_{150}O_\eta}\cdots\mathrm{Tyr_{150}H_\eta}$ and $\mathrm{Lys_{67}N_\zeta}\cdots\mathrm{Tyr_{150}H_\eta}$ during the metadynamics simulation of acylation of cephalothin as discussed in Section 3.3 of the manuscript. This shows that $\mathrm{Tyr_{150}H_\eta}$ has been transferred between $\mathrm{Tyr_{150}O_\eta}$ and $\mathrm{Lys_{67}N_\zeta}$ several times during the simulation, indicating that both **KY:Cep** as well as $\mathbf{K^+Y^-}$**:Cep** configurations were sampled. The dotted line at 1.2 Å is to easily gauge the protonation state.

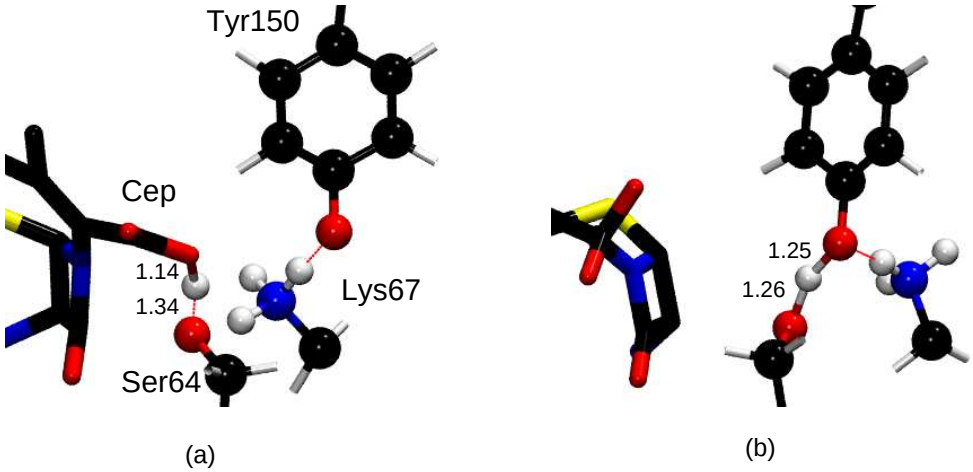

Fig SI 14: Two crucial configurations observed during the metadynamics simulation where $Ser_{64}H_{\gamma}$ transferred to (a) carboxylate group of Cep, and (b) $Tyr_{150}O_{\eta}$. More details are present in Section 3.3 of the manuscript.

References

[1] C. Oefner, A. D'Arcy, J. J. Daly, K. Gubernator, R. L. Charnas, I. Heinze, C. Hubschwerlen, and F. K. Winkler, *Nature*, **1990**, *343*, 284–288.

[2] G.Schaftenaar and J.H. Noordik, *J. Comput.-Aided Mol. Design*, **2000**, *14*, 123–134.

[3] M. J. Frisch, G. W. Trucks, H. B. Schlegel, G. E. Scuseria, M. A. Robb, J. R. Cheeseman, G. Scalmani, V. Barone, B. Mennucci, G. A. Petersson, H. Nakatsuji, M. Caricato, X. Li, H. P. Hratchian, A. F. Izmaylov, J. Bloino, G. Zheng, J. L. Sonnenberg, M. Hada, M. Ehara, K. Toyota, R. Fukuda, J. Hasegawa, M. Ishida, T. Nakajima, Y. Honda, O. Kitao, H. Nakai, T. Vreven, Jr. J. A. Montgomery, J. E. Peralta, F. Ogliaro, M. Bearpark, J. J. Heyd, E. Brothers, K. N. Kudin, V. N. Staroverov, T. Keith, R. Kobayashi, J. Normand, K. Raghavachari, A. Rendell, J. C. Burant, S. S. Iyengar, J. Tomasi, M. Cossi, N. Rega, J. M. Millam, M. Klene, J. E. Knox, J. B. Cross, V. Bakken, C. Adamo, J. Jaramillo, R. Gomperts, R. E. Stratmann, O. Yazyev, A. J. Austin, R. Cammi, C. Pomelli, J. W. Ochterski, R. L. Martin, K. Morokuma, V. G. Zakrzewski, G. A. Voth, P. Salvador, J. J. Dannenberg, S. Dapprich, A. D. Daniels, O. Farkas, J. B. Foresman, J. V. Ortiz, J. Cioslowski, and D. J. Fox.; *Gaussian 09, Revision B.01;* Gaussian, Inc., Wallingford CT, 2010;
see also `http://www.gaussian.com/` .

[4] J. C. Gordon, J. B. Myers, T. Folta, V. Shoja, L. S. Heath, and A. Onufriev, *Nucleic Acids Res.*, **2005**, *33*, W368–W371,
see also `http://biophysics.cs.vt.edu/credits.php` .

[5] Y. Zhao and D. G. Truhlar, *Theo. Chem. Acc.*, **2008**, *120*, 215–41.